Aerospace Science and Technology 45 (2015) 39–49

Contents lists available at ScienceDirect

Aerospace Science and Technology

www.elsevier.com/locate/aescte

Effects of aerodynamic modeling on the optimal wing kinematics for hovering MAVs

Zhimiao Yan [a,*,1], Haithem E. Taha [b,2], Muhammad R. Hajj [a,3]

[a] Department of Biomedical Engineering and Mechanics, Virginia Tech, Blacksburg, VA 24061, USA
[b] Department of Mechanical and Aerospace Engineering, University of California Irvine, Irvine, CA 92697-3975, USA

ARTICLE INFO

Article history:
Received 19 December 2014
Received in revised form 18 April 2015
Accepted 20 April 2015
Available online 23 April 2015

Keywords:
Anti-optimization
Flapping flight
Hovering insects
Optimum kinematics
Unsteady modeling

ABSTRACT

The effects of aerodynamic model assumptions on the optimal wing-kinematics for hovering micro-air-vehicles are determined. Specific kinematic functions for the wing motion are specified and the parameters of these functions are considered as the design variables for the optimization problem. Four aerodynamic models having different levels of fidelity that capture various physical aspects of hovering aerodynamics are considered to assess the effects of these different aspects on the optimal wing kinematics. These physical aspects include the leading edge vortex, rotational lift, non-circulatory contributions, and flow unsteadiness. Conventional models for pitching wings are not adequate as they predict considerably high rotational lift and too little power requirements, which makes the optimizer, unrealistically, leans toward almost pure rotational motion with little flapping. In addition, quasi-steady modeling overestimates the generated lift and, as such, leads to a more optimal, but unrealistic, performance. Therefore efficient unsteady modeling is essential in design optimization of flapping-wing micro-air-vehicles.

1. Introduction

The stringent weight and power constraints, imposed by design specifications of micro-air-vehicles (MAVs), present the need for optimal design and performance. As such, there is a strong interest in determining optimal wing shapes, wing flapping kinematics, and actuation mechanisms. This work is concerned with optimization of the flapping kinematics. These kinematics are usually described by three Euler angles relating the wing axes x, y, and z to the body axes X, Y and Z, namely, the back and forth flapping angle φ, the plunging angle ϑ, and the pitching angle η. Taha et al. [22] identified two common frameworks within which optimal time variations of these Euler angles are sought. In the first framework, specific patterns along with associated parametrization for the kinematic functions are sought to achieve high control authority for the MAV, see Schenato et al. [20], Doman et al. [9], and Oppenheimer et al. [17]. One exception is the work of Taha et al. [23] who used the calculus of variations to analytically determine the maximum acceleration that a flapping MAV can ever attain from the hovering position using a horizontal stroke plane. In the second framework, the wing kinematics are optimized from the aerodynamic performance point of view. The present work lies within the latter framework.

Berman and Wang [3] considered the optimization of the wing Euler angles with respect to the body for hovering insects, namely, the hawk moth, bumble bee, and fruit fly. They proposed specific functional forms and kinematic parametrization (11 parameters) for the three Euler angles that sweep a very wide family of functions. They used the quasi-steady aerodynamic model developed by Pesavento and Wang [18] and Andersen et al. [1,2]. This model accounts for the translatory (leading edge vortex), rotational, viscous, and added mass effects. Berman and Wang used both gradient-based and global optimization techniques to minimize the average required power (aerodynamic + inertial) under the lift constraint that lift is equal weight. Kurdi et al. [16] considered the same problem of wing kinematics optimization to minimize the required hovering power. They used the quasi-steady aerodynamic model of Pesavento and Wang [18] and Andersen et al. [1,2]. However, they adopted a different approach for optimization of the shapes of the kinematic functions. They used 30 design variables for each Euler angle to specify the magnitudes of each angle at specific instants during the flapping cycle. Spline interpolation was then performed to obtain differentiable functions. Kurdi

* Corresponding author.
E-mail addresses: t850905@vt.edu (Z. Yan), hetaha@uci.edu (H.E. Taha), mhajj@vt.edu (M.R. Hajj).
[1] Post-doctoral research fellow.
[2] Assistant professor.
[3] Professor.

http://dx.doi.org/10.1016/j.ast.2015.04.013
1270-9638/

Nomenclature

$\mathcal{AR}$	Aspect ratio
c	Chord length
C_L	Lift coefficient
C_D	Drag coefficient
C_{Df}	Skin friction drag contribution
d_{LEV}	Two-dimensional translational drag force
d_{NC}	Two-dimensional non-circulatory drag force
f	Flapping frequency
L	Total lift force
ℓ	Two-dimensional lift force
L_{LEV}	Total translational lift force
ℓ_{LEV}	Two-dimensional translational lift force
L_{NC}	Total non-circulatory lift force
ℓ_{NC}	Two-dimensional non-circulatory lift force
L_{ROT}	Total rotational lift force
m_{app}	Apparent mass of the two-dimensional strip
N_{NC}	Two-dimensional non-circulatory normal force
P_{areo}	Total aerodynamic power
$P_{aero,LEV}$	Aerodynamic power due to translational effects
$P_{inertial}$	Inertial power
P_{mech}	Required mechanical power
P_{NC}	Non-circulatory aerodynamic power
U	Forward free-stream velocity
$W(s)$	Wagner function
x, y, z	Local coordinate fixed on wing axes
X, Y, Z	Global coordinate fixed on body
α	Angle of attach
η	Pinching angle
ϑ	Plunging angle
Γ_{QS}	Quasi-steady circulation
Φ_η	Phase angle between flapping and pitching
ρ	Density of the air
φ	Back and forth flapping angle

et al. used gradient-based algorithms for their optimization problem. They also determined the effect of the levels of elastic storage and cost to dissipate negative power on the optimization problem. The elastic storage was modeled as a fraction of the inertial power and the remaining inertial power was modeled as a dissipation cost.

Stanford and Beran [21] performed a gradient-based optimization of flapping-wing active-shape-morphing in forward flight. They performed a sensitivity analysis using the three-dimensional unsteady vortex-lattice method to obtain the gradient of their objective function with respect to the design variables. Their objective was to maximize the aerodynamic efficiency under lift and thrust constraints. They represented the wing morphing along with the flapping motions by a finite series of spatial and temporal functions. The spatial functions are the first twisting and bending modes of the wing. As for the design variables, they adopted two techniques. The first technique assumes harmonic functions for the time variation of the generalized coordinates and, as such, the design variables were the amplitudes and phase shifts of the generalized coordinates. The second technique is similar to that of Kurdi et al. [16], in which the time variations of the kinematic functions were approximated by cubic splines and the amplitudes of the generalized coordinates at specific control points represented the design variables. Ghommem et al. [14] adopted the same approaches using global and hybrid (global and gradient-based) optimization techniques.

All of the efforts on the aerodynamic optimization of flapping wing kinematics discussed above have adopted finite-dimensional optimization. Taha et al. [24] were the first to formulate the problem as an infinite dimensional one; i.e., a calculus of variations problem. They used a quasi-steady aerodynamic model accounting for the leading edge vortex effect and showed that the triangular waveform along with a piece-wise constant pitch angle resulted in hovering with minimum power.

The problem of wing-kinematic optimization for hovering MAVs is considered. Following Ellington [10] and Weis-Fogh [31], a horizontal stroke plane ($\vartheta = 0$) is assumed. The shape of the kinematic functions proposed by Berman and Wang [3] for the two Euler angles φ and η is adopted with the same parametrization. The parameters in these kinematic functions are considered as the design variables for the optimization problem. The performance index to be minimized is the hovering aerodynamic power. The main contribution of this work is to determine the effects of the aerodynamic model on the optimal wing kinematics. First, a quasi-steady representation of the dominant leading-edge vortex effect is used. Second, the rotational lift is added. Third, the non-circulatory contributions are added. Finally, a full unsteady model that accounts for all of these aspects in the unsteady representation developed by Taha et al. [25] is used. As such, the specific impact of each aerodynamic effect on the optimal wing-kinematics is assessed. This study also serves as an anti-optimization tool for the aerodynamic modeling of flapping flight. That is, since the optimizer usually seeks the flaws in the used model, the optimizer would tell about any un-clear/un-expected flaws in a specific aerodynamic model of flapping flight.

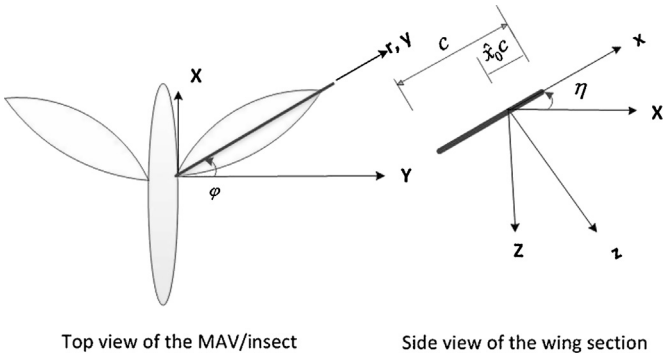

Fig. 1. A schematic of the insect.

2. Kinematic model

In this work, the optimization of the wing kinematics is considered through optimizing the waveforms of two Euler angles; the flapping (azimuth) angle φ and the pitching angle η. Fig. 1 shows a schematic diagram for a hovering micro-air-vehicle. The kinematic functions and parametrization proposed by Berman and Wang [3] are used. As such, the azimuthal angle (φ) and pitching angle (η) are written as:

$$\varphi(t) = \frac{\varphi_m}{\sin^{-1} K}\sin^{-1}[K\sin(2\pi f t)]$$
$$\eta(t) = \frac{\eta_m}{\tanh C_\eta}\tanh[C_\eta \sin(2\pi f t + \Phi_\eta)] + \eta_0 \qquad (1)$$

where, φ_m and η_m are the amplitudes of the flapping and pitching angles, respectively, K and C_η are controlling parameters for the flapping and pitching angle, respectively, f is the flapping

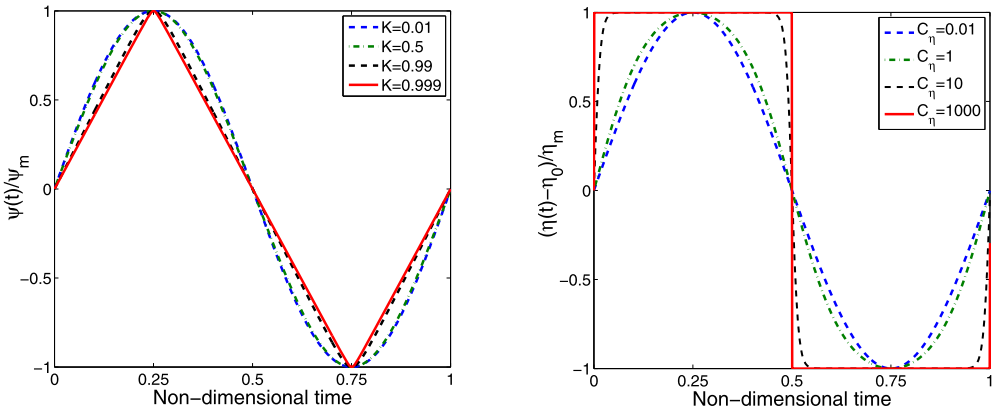

(a) Variation of φ with K. (b) Variation of η with C_η.

Fig. 2. Variations of the shapes of the flapping and pitching angles as K varies from 0 to 1 and C_η varies from 0 to ∞, respectively.

frequency, Φ_η is the phase angle between flapping and pitching, and η_0 is the mean pitching angle. Fig. 2 shows the variations of the shapes of the flapping and pitching angles as K varies from 0 to 1 and C_η varies from 0 to ∞, respectively. The waveform of $\varphi(t)$ approaches a sinusoidal waveform as $K \to 0$ and a triangular waveform as $K \to 1$. As for the pitching waveform, $\eta(t)$ approaches a sinusoidal waveform as $C_\eta \to 0$ and a step function as $C_\eta \to \infty$ [3]. These seven parameters for the kinematic functions are considered as the design variables for the optimization problem.

3. Aerodynamic models

For several decades, insect flight has been considered impossible from the classical aerodynamics point of view. Biologists who initiated the interest in analyzing insect flight were able to calculate the required lift coefficient to support an insect's weight. The calculated lift coefficients are considerably higher than those seen in classical aerodynamics at the low Reynold's numbers of interest. Therefore, almost all of the early trials (e.g., [6,7]) invoked unconventional lift mechanisms. Dickinson et al. [8] presented three unconventional mechanisms for lift generation that are exploited by insect flight, namely, the leading edge vortex (LEV) effects, the rotational effects, and the wake capture effects.

3.1. Quasi-steady models

3.1.1. Translation (leading edge vortex effect)

The LEV contribution to lift is the dominant one in insect flight. The LEV augments the circulation in the flow and, as such, increases the generated lift force. It should be noted that this process is similar to what happens in a dynamic stall situation where a rapid change in the angle of attack leads to the creation of a LEV that enhances the lift at the beginning. However, the generated LEV in dynamic stall is unstable. That is, it sheds with the flow after a while and causing a large pitching down moment followed by a complete flow separation when the vortex leaves the wing trailing edge. Luckily, for flapping flight, similar to highly swept and delta wings and propeller and helicopter blades, the LEV has stable characteristics; i.e., it remains attached to the wing surface. Using flow visualization, Ellington et al. [12] and Van den Berg and Ellington [28,29] have shown that the stability characteristics of the LEV in insect flight is due to a spanwise flow because of the spanwise pressure gradient due to the rotational motion of the wing about the fulcrum. It is the same stabilizing mechanism in propeller and helicopter blades.

In this subsection, the dominant contribution of the aerodynamics of hovering insects is considered; that is, the LEV effect. The lift force on a translational wing is expressed as:

$$\ell_{LEV} = \frac{1}{2}\rho U^2 c C_L \tag{2}$$

where ρ is the air density, c is the chord length, C_L is the lift coefficient, and U is the forward free-stream velocity. Since pitching plane flapping is considered in this work, $U = r\dot{\varphi}$, and the angle of attack α is related to the pitching angle via

$$\alpha(t) = \begin{cases} \eta, & \dot{\varphi} > 0 \\ \pi - \eta, & \dot{\varphi} < 0 \end{cases}$$

The lift coefficient due to a stabilized LEV is given in [30] as

$$C_L = A \sin 2\alpha \tag{3}$$

where, according to Taha et al. [25], $A = \frac{C_{L_\alpha}}{2}$ and

$$C_{L_\alpha} = \frac{\pi \mathcal{AR}}{1 + \sqrt{(\frac{\pi \mathcal{AR}}{a_0})^2 + 1}} \tag{4}$$

where a_0 is the lift curve slope of the two-dimensional airfoil section (taken here to be 2π), $\mathcal{AR}$ is the aspect ratio of one wing $\mathcal{AR} = \frac{R^2}{S}$, R is the wing length and S is the wing area. As such, the total translational lift force is written as:

$$L_{LEV} = \frac{1}{2}\rho A I_{21} \dot{\varphi}^2 \sin 2\alpha \tag{5}$$

where, $I_{mn} = 2\int_0^R r^m c^n(r) dr$

The drag coefficient due to a stabilized LEV is written as $C_D = C_L \tan\alpha$ [19]. Then, a skin friction drag contribution, C_{D_f}, should be added, which yields

$$C_D = 2A \sin^2\alpha + C_{D_f} \tag{6}$$

Thus, the translational drag force is written as:

$$d_{LEV} = \frac{1}{2}\rho U^2 c (2A \sin^2\alpha + C_{Df}) \tag{7}$$

Then, the aerodynamic power due to translational effects (LEV and skin friction) only is calculated as:

$$P_{aero,LEV} = 2\int_0^R d_{LEV}|U| dr = \frac{1}{2}\rho I_{31} |\dot{\varphi}| \dot{\varphi}^2 (2A \sin^2\alpha + C_{Df}) \tag{8}$$

3.1.2. Rotational lift

In this model, the effects of wing rotation (pitching) are included. According to the potential flow theory, a pitching airfoil creates a rotational circulation that is given by $\Gamma_{rot} = \pi c^2 \dot{\alpha}(\frac{3}{4} - \hat{x}_0)$ [13], where $\hat{x}_0$ is the chord-normalized distance from the leading edge to the hinge axis. Since a horizontal stroke plane is considered, this circulation induces additional lift on the flapping wing. Therefore, the rotational lift force is written as:

$$L_{ROT} = \int_0^R 2\rho U \pi c^2 \dot{\alpha}(\frac{3}{4} - \hat{x}_0))dr = \pi \rho I_{12}(\frac{3}{4} - \hat{x}_0)\dot{\varphi}\dot{\alpha} \tag{9}$$

Because potential flow theory is considered to model the contribution of wing rotation, there is no resulting drag force. As such, the aerodynamic power can be calculated from Eq. (8) when both LEV and rotational effects are considered.

3.1.3. Non-circulatory loads

In this subsection, the non-circulatory (added mass) contributions are accounted for. Although the non-circulatory loads are unsteady loads, they are included here in the quasi-steady section because they are represented by algebraic expressions in terms of the instantaneous wing speed and acceleration. So, there are no flow dynamics needed to determine such loads. It is assumed that only accelerations perpendicular to the wing chord (plunging-like) generate non-circulatory normal forces. The acceleration of the hinge point, normal to the wing chord, induced by the flapping motion, is written as

$$a_y(r,t) = r[-\ddot{\varphi}(t)\sin\eta(t) - \dot{\varphi}(t)\dot{\eta}(t)\cos\eta(t)] \tag{10}$$

Then, the produced non-circulatory normal force is written as [4]

$$N_{NC}(r,t) = -m_{app}(r)a_y(r,t) \tag{11}$$

where $m_{app}(r) = \frac{\pi}{4}\rho c^2(r)$ is the apparent mass of the two-dimensional strip. As such, the non-circulatory incremental lift and drag forces are calculated as

$$\begin{aligned}\ell_{NC} &= N_{NC}\cos\eta = \frac{\pi\rho c^2}{4}[r\ddot{\varphi}\sin\eta + r\dot{\varphi}\dot{\eta}\cos\eta]\cos\eta \\ d_{NC} &= N_{NC}\sin\eta sign(\dot{\varphi}) \\ &= \frac{\pi\rho c^2}{4}[r\ddot{\varphi}\sin\eta + r\dot{\varphi}\dot{\eta}\cos\eta]\sin\eta sign(\dot{\varphi})\end{aligned} \tag{12}$$

Thus, non-circulatory lift can be calculated as:

$$L_{NC} = \frac{\pi}{4}\rho I_{12}(\ddot{\varphi}\sin\eta + \dot{\varphi}\dot{\eta}\cos\eta)\cos\eta \tag{13}$$

The non-circulatory power requirement includes two contributions; a translatory component and a rotational component. These two components are given by:

$$P_{NC} = 2\int_0^R d_{NC}|U|dr + 2\int_0^R I_a\ddot{\eta}\dot{\eta}dr \tag{14}$$

where $I_a = \frac{1}{128}\pi\rho c^4$ is the added inertia. Thus, the integrated non-circulatory power requirements are written as

$$P_{NC} = \frac{1}{128}\pi\rho I_{04}\ddot{\eta}\dot{\eta} + \frac{\pi}{4}\rho I_{22}(\dot{\varphi}\ddot{\varphi}\sin\eta + \dot{\varphi}^2\dot{\eta}\cos\eta)\sin\eta \tag{15}$$

3.2. Full unsteady aerodynamic model

In this model, a full unsteady representation of the aerodynamic lift that accounts for all of the previous physical aspects in an unsteady fashion is used. Taha et al. [26,25] developed an aerodynamic model that captures the nonconventional lift mechanism (due to LEV) in an unsteady formulation. It also captures the rotational lift in the same way. Finally, the non-circulatory loads can be added to the obtained circulatory part. This model is based on the two-state approximation to the Wagner function, by Jones [15], of the form

$$W(s) = 1 - A_1 e^{-b_1 s} - A_2 e^{-b_2 s} \tag{16}$$

where s is the non-dimensional time. Taha et al. [25] obtained the aerodynamic response (lift) due to any arbitrary varying aerodynamic input using Duhamel's superposition principle. They showed that the appropriate aerodynamic input that should be used in Duhamel's principle is the quasi-steady circulation. As such, they provided a means to account for nonconventional lift mechanisms (arbitrary lift curves) in an unsteady fashion.

Taha et al. [25] modelled the total lift on the two-dimensional airfoil section as

$$\ell = \ell_{NC} + \rho U(t)[\Gamma_{QS}(t)W(0) - \int_0^t \Gamma_{QS}(\tau)\frac{dW(t-\tau)}{d\tau}d\tau] \tag{17}$$

where, Γ_{QS} is the quasi-steady circulation that is written as

$$\Gamma_{QS} = \frac{1}{2}UcC_L(\alpha) + \pi c^2\dot{\alpha}(\frac{3}{4} - \hat{x}_0)$$

where $C_L(\alpha) = A\sin 2\alpha$ for a stabilized LEV. Through some mathematical manipulation, they showed that

$$\ell = \ell_{NC} + \rho U(r,t)[(1 - A_1 - A_2)\Gamma_{QS}(r,t) + x_1(r,t) + x_2(r,t)] \tag{18}$$

where, $x_i(r,t)$ are aerodynamic internal states whose dynamics are described by

$$\dot{x}_i(r,t) = \frac{2b_i U(r,t)}{c}(-x_i(r,t) + A_i\Gamma_{QS}(r,t))$$

where, according to Jones [15], the values of the coefficients A_1, A_2, b_1 and b_2 are, respectively, equal to 0.165, 0.335, 0.0455 and 0.3.

According to the above model, if 50 spanwise stations are used, a total of 100 aerodynamic states would be required. To be more suitable for optimization and sensitivity analyses, Taha et al. [25] proposed a fourth order model that still captures the same physical aspects (LEV, unsteadiness, and rotational contributions). They developed this model by exploiting the knowledge of the spanwise distributions of all the lift contributors in the integration of Eq. (18) over the wing. This dictates the separation of the translational term from the rotational one because the two terms have different spanwise distributions: $r^2c(r)$ for the translational term versus $rc^2(r)$ for the rotational term. As such, the total lift on the wing is written as $L = L_{NC} + L_{trans} + L_{rot}$ where

$$\begin{aligned}L_{NC}(t) &= \frac{\pi}{4}\rho I_{12}[\ddot{\varphi}(t)\sin\eta(t) + \dot{\varphi}(t)\dot{\eta}(t)\cos\eta(t)]\cos\eta(t) \\ L_{trans}(t) &= \frac{1}{2}\rho I_{21}|\dot{\varphi}(t)|[(1 - A_1 - A_2)\dot{\varphi}(t)C_L(\eta(t)) + x_1(t) \\ &\quad + x_2(t)]\end{aligned} \tag{19}$$

and

$$L_{rot}(t) = \rho I_{12}(\frac{3}{4} - \widehat{x}_0)\dot{\varphi}(t)[(1 - A_1 - A_2)\dot{\eta}(t) + x_3(t) + x_4(t)]$$

and the state equations for the four states are given by

$$\dot{x}_i(t) = \frac{2b_j\bar{r}|\dot{\varphi}(t)|}{\bar{c}}\left[-x_i(t) + A_j\dot{\varphi}(t)C_{L,s}(\eta(t))\right], \quad j = i = 1,2$$
$$\dot{x}_i(t) = \frac{2b_j\bar{r}|\dot{\varphi}(t)|}{\bar{c}}\left[-x_i(t) + A_j\dot{\eta}(t)\right], \quad j = i-2 = 1,2 \qquad (20)$$

where $\bar{r}$ and $\bar{c}$ are taken at a certain reference section and $C_{L,s}$ is quasi-steady lift coefficient. In this study, the section at $r = r_2 = \frac{I_{21}}{2SR}$ is used as a reference section.

As for the drag force, it is calculated as $D = (L_{NC} + L_{trans})\tan\alpha + D_f$, where D_f is the skin friction drag. Thus, the total aerodynamic power is calculated as:

$$P_{areo} = \left(\frac{I_{31}}{I_{21}}L_{trans} + \frac{I_{22}}{I_{12}}L_{NC}\right)\tan\alpha + \frac{1}{2}\rho I_{31}C_{Df}\,|\dot{\varphi}|\,\dot{\varphi}^2 + \frac{1}{16}\pi\rho I_{04}(\mu_1 f + \mu_2|\dot{\eta}|)\dot{\eta}^2 \qquad (21)$$

It should be noted that the selected aerodynamic model is a reduced-order one that captures the large-scale quantities (loads) with a good accuracy, as shown by the comparisons with Navier–Stokes solutions presented in Ref. [25]. This is quite suitable for an efficient solution to the optimization problem. However, it would be quite interesting to investigate the vortex structure generated by the optimum kinematics.

4. Power optimization

The total mechanical power required to ensure the desired kinematics comprises aerodynamic and inertial contributions. The first component has been presented in the previous section in each aerodynamic model. The inertial power is given by

$$P_{inertia}(t) = 2I_z\ddot{\varphi}\dot{\varphi} + 2I_y\ddot{\eta}\dot{\eta} \qquad (22)$$

where I_z and I_y are the moments of inertia about the z axis and y axis, respectively. Kurdi et al. [16] represented all the combinations of the required mechanical power as follows:

$$P_{mech} = \begin{cases} -\alpha|P_{mech}| + \beta(1-\alpha)|P_{mech}|, & P_{mech} < 0 \\ P_{mech}, & P_{mech} \geq 0 \end{cases} \qquad (23)$$

where α and β represent the percentages of the elastic storage and the cost to dissipate negative power, respectively. For $\alpha = 1$, the system is assumed to have 100% elastic storage. On the other hand, $\alpha = 0$ indicates that the system has no elastic storage and β comes to play a role. For $\beta = 0$, there will be no cost to dissipate negative power, while $\beta = 1$ indicates that 100% cost is paid to dissipate negative power. Weis-Fogh [31] concluded that insects must have elastic storage, otherwise they will not be able to metabolically sustain flight. Also, it is quite practical to design a MAV with an elastic storage (a spring element in the stroke plane). As such α is set to 1 in this work (i.e., 100% elastic storage is considered).

The optimization problem is then stated as follows

$$\min_{\chi} \bar{p}*_{mech} = \frac{1}{MT}\int_0^T P_{mech}(t)dt \quad \text{subject to}$$
$$\bar{L}* = \frac{1}{MT}\int_0^T L(t)dt \geq g \text{ and } \chi_{LB} < \chi < \chi_{UB}$$

where M is the mass of the vehicle, g is the gravitational acceleration and the vector χ of design variables includes the seven kinematic parameters $\chi = [\varphi_m, \mathrm{K}, \mathrm{f}, \eta_m, \mathrm{C}_\eta, \mathbf{\Phi}_\eta, \eta_0]^T$ and χ_{LB} and χ_{UB} are its lower and upper bounds, respectively.

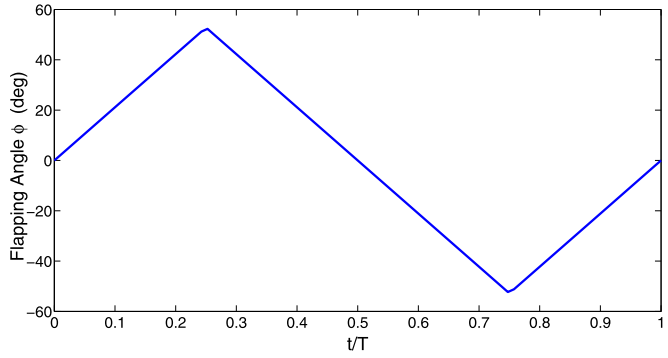

(a) Optimum flapping angle φ

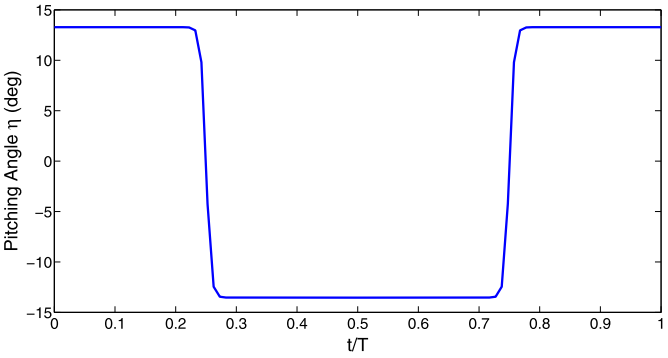

(b) Optimum pitching angle η

Fig. 3. Optimal kinematic functions using the LEV contribution only.

The hawkmoth is considered as a case study in this work. Its morphological parameters, as provided by Ellington [11], are given by

$$R = 51.9 \text{ mm}, \bar{c} = 18.26 \text{ mm and } S = 947.8 \text{ mm}^2$$

For the wing shape, elliptic chord-distributions are assumed on the form

$$c(r) = \frac{4\bar{c}}{\pi}\sqrt{1 - \frac{r^2}{R^2}} \qquad (24)$$

where, $\bar{c}$ is the mean chord length of the wing. The friction drag coefficient C_{D_f} of the hawkmoth is assumed to be 0.07 [3].

5. Results and discussion

Fig. 3 shows the optimal wing kinematics using the quasi-steady representation of the LEV only. The optimal kinematics asymptotically reach the results obtained by Taha et al. [24] using calculus of variations; a triangular waveform for the back and forth flapping angle along with piece-wise constant variation for the pitching angle. Moreover, the value of the constant angle of attack η_0 is the one that minimizes $\frac{C_D^2}{C_L^3}$ as shown in Fig. 4. This result is also consistent with the analytical result of Taha et al. [24].

Fig. 5 shows the optimal kinematics obtained by using the LEV and rotational models described before. The optimizer is totally dependent on the rotational motion as a cheap source of producing lift. This is concluded from the 7° flapping amplitude and the 180° pitching amplitude. Moreover, during the translational phase, the angle of attack is almost zero which can be found form the expression of angle of attack α and Fig. 5(b). The optimizer required this translational motion just to attain some forward speed because the rotational lift is proportional to U. After attaining an appropriate U, the wing flips instantaneously with a very large pitching angular velocity to achieve the required lift. These conclusions are

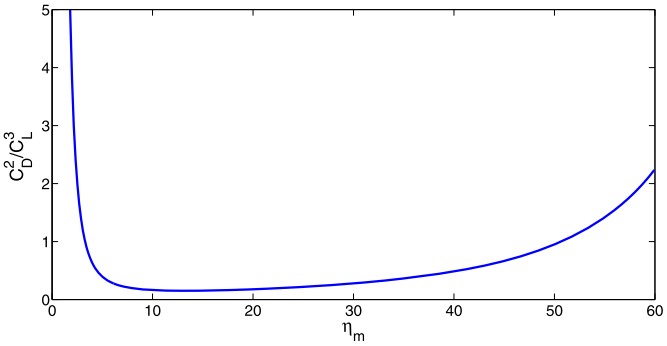

Fig. 4. Performance index C_D^2/C_L^3 versus the angle of attack.

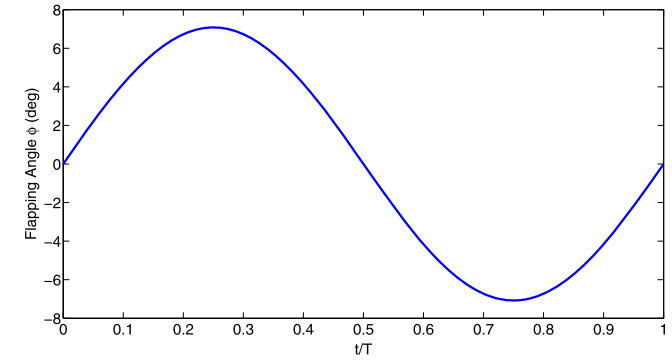

(a) Optimum flapping angle φ

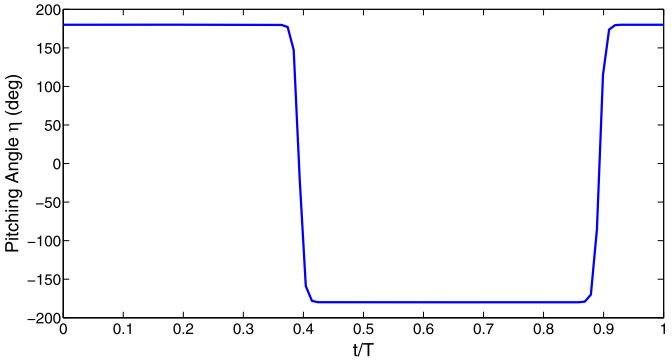

(b) Optimum pitching angle η

Fig. 5. Optimal kinematic functions using the LEV and rotational contributions without considering the viscous effect.

supported by Fig. 6, which shows the LEV and rotational contributions of the lift and power variations over the flapping cycle. The zero rotational contribution to the required power and the zero LEV contribution to the generated lift are clear in Fig. 6.

The common assumption of neglecting the rotational drag contribution may be justifiable relative to the translational one. However, this is the reason that the optimizer finds the rotational motion as a Utopian choice; producing lift at no cost. So, the optimal kinematics is pure rotation without a considerable translation. This is what is usually referred to as *anti-optimization*; that is by performing optimization, one is able to discover the flaws in the used aerodynamic model as the optimizer usually points to the weaknesses in the adopted model. To prevent that, the rotational viscous friction model proposed by Berman and Wang [3] is adopted. As such, the viscous torque is written as

$$\tau_f = -\frac{1}{16}\pi\rho_{air}c^4(r)\left[\mu_1 f + \mu_2|\dot{\eta}|\right]\dot{\eta} \tag{25}$$

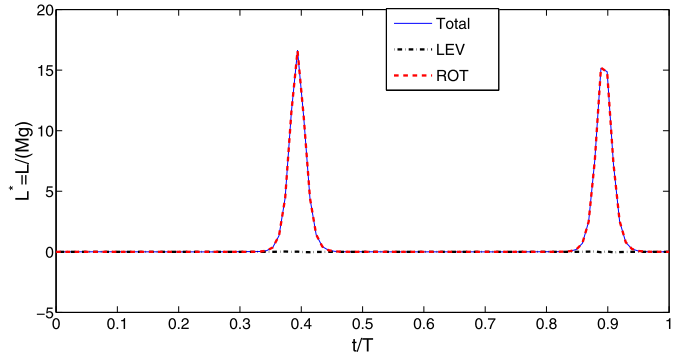

(a) Lift-to-weight

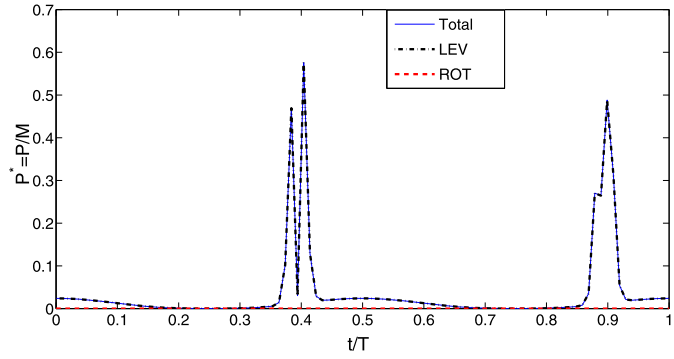

(b) Normalized power P^*

Fig. 6. Optimal kinematic functions using the LEV and rotational contributions without considering the viscosity.

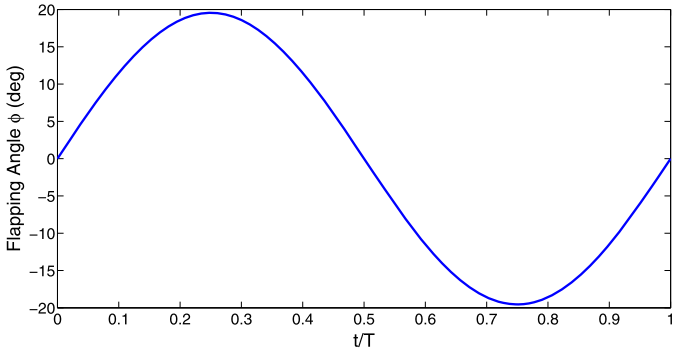

(a) Optimum flapping angle φ

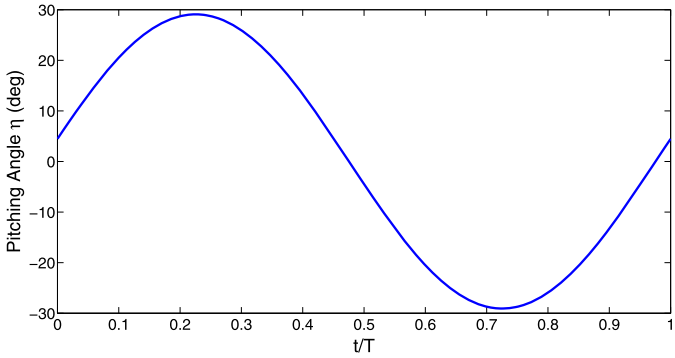

(b) Optimum flapping angle η

Fig. 7. Optimal kinematic functions using the LEV and rotational contributions.

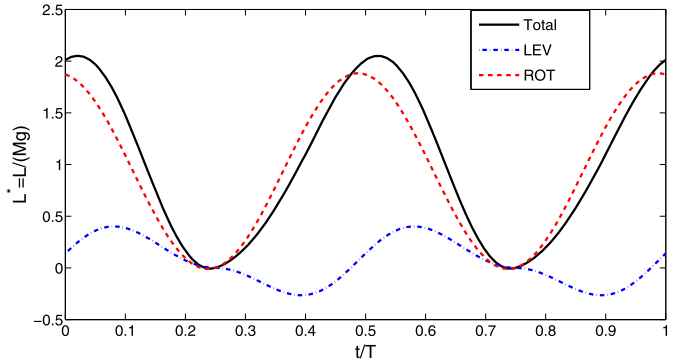

(a) Lift-to-weight

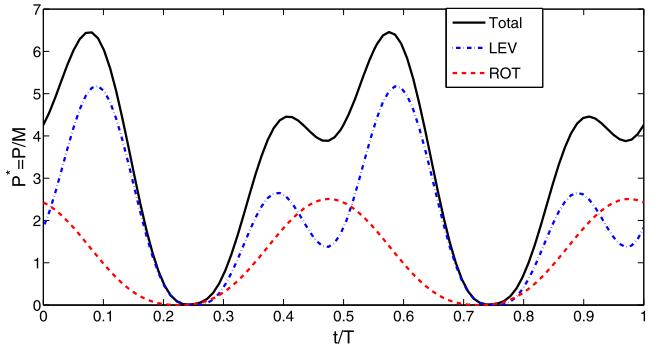

(b) Normalized power P^*

Fig. 8. Optimal kinematic functions using the LEV and rotational contributions.

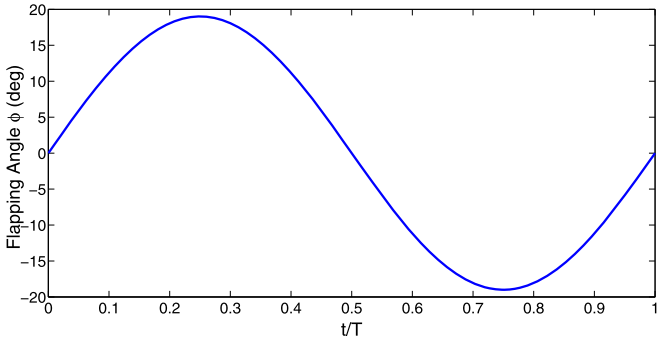

(a) Optimum flapping angle φ

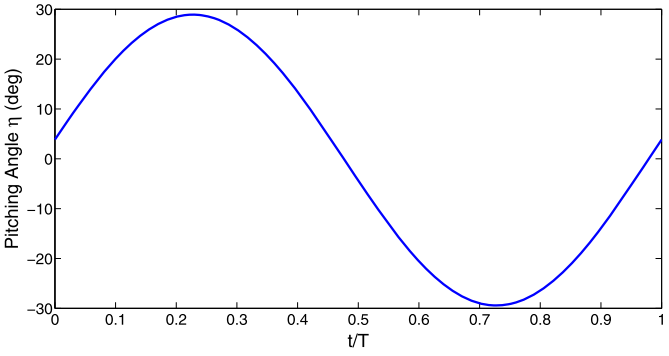

(b) Optimum flapping angle η

Fig. 9. Optimal kinematic functions using full quasi-steady representation: LEV, rotational, and non-circulatory contributions.

where, μ_1 and μ_2 are dimensionless coefficients related to the viscosity of the fluid and f is the flapping frequency. Berman and Wang recommended a value of 0.2 for both of them. Thus, the aerodynamic power required to overcome the viscous rotational damping is given by

$$P_{ROT} = -2\int_0^R \tau_f \dot{\eta} dr = \frac{1}{16}\pi\rho l_{04}(\mu_1 f + \mu_2 |\dot{\eta}|)\dot{\eta}^2 \tag{26}$$

Incorporating these viscous effects into the model for rotational contributions, more reasonable kinematics are obtained. In comparison with the results of the LEV only, the parameters controlling the shapes of the kinematic functions show a significant change. The value of K changes from its maximum value (unity) to zero and that of C_η changes from ∞ to zero, leading to smoother functions, as shown in Fig. 7. However, because the adopted model for rotational effects did not induce any drag force and, consequently, power consumption other than the rotational viscous power in Eq. (26), the optimizer is still leaning and depending on rotational motion as shown in Figs. 7 and 8. This is because the rotational motion creates lift with very low power consumption in comparison to the translational motion. As such, the optimum flapping amplitude φ_m decreases considerably from 52.8° to 19.5° and the pitching amplitude increases from 13.4° to 29.1°, as shown in Table 1. As a result, hovering is achieved with much less power; the optimum mass-normalized power is reduced from 19.52 W/kg to 3.22 W/kg.

Adding the non-circulatory components does not lead to a considerable change in the optimal kinematics, as shown in Figs. 9 and 10. This result is intuitively expected because the non-circulatory (added mass) components are considered like inertial loads which, in the optimization problem at hand, do not contribute to the averaged power consumption. 100% elastic storage is assumed.

Using the full unsteady model results in some deviation for the optimal flapping kinematics and power consumption, as shown in Fig. 11. It is important to note that the unsteady effects lead to an optimum mass-normalized power of 6.31 W/kg versus 3.06 W/kg for the full quasi-steady model. This result indicates that optimization of flapping kinematics using quasi-steady aerodynamics may lead to less conservative results. This is because quasi-steady models over-estimate the produced lift forces, while the unsteady counterparts capture the lift deficiency [4,5], e.g., the Theodorsen function (the lift deficiency factor) [27]. Taha et al. [26] showed that hovering insects operate in the frequency range of maximum

Table 1
Optimal parameters for the kinematic functions describing the wing motion and the corresponding minimum average aerodynamic power ($\bar{P}^*_{mech}$).

Parameters	LEV	LEV and inviscid rotation	LEV and viscous rotation	Full quasi-steady	Full unsteady
f (Hz)	46.07	35.31	50.00	50.00	50.00
φ_m°	52.82	7.08	19.54	18.99	25.48
η_m°	13.41	179.97	29.07	29.16	35.87
η_0°	−0.13	0.0011	0.0031	−0.25	−0.15
K	0.99	0.051	0.01	0.01	0.01
C_η	20.00	10.00	0.0096	0.0090	0.0080
Φ_η°	90.00	38.52	8.85	8.079	12.64
$\bar{P}^*_{mech}$(W/kg)	19.52	0.037	3.22	3.06	6.32

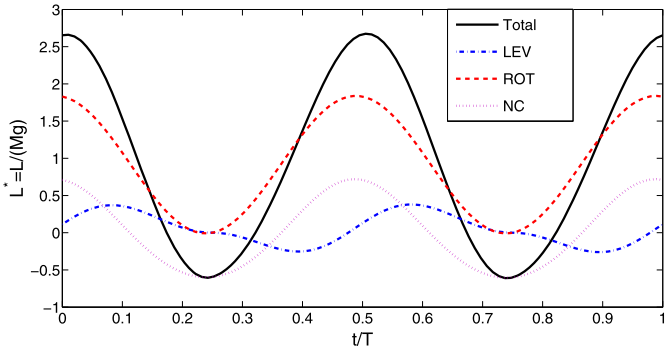

(a) Lift-to-weight

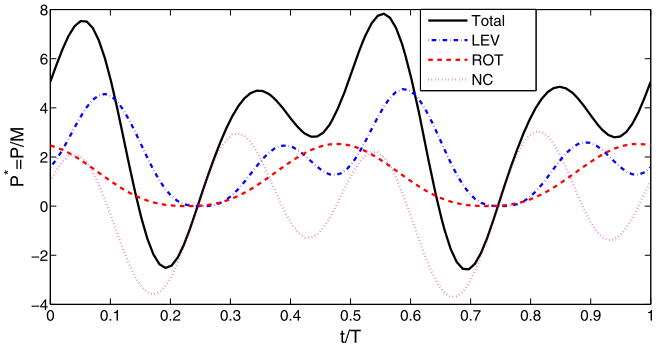

(b) Normalized power P^*

Fig. 10. Optimal kinematic functions using full quasi-steady representation: LEV, rotational, and non-circulatory contributions.

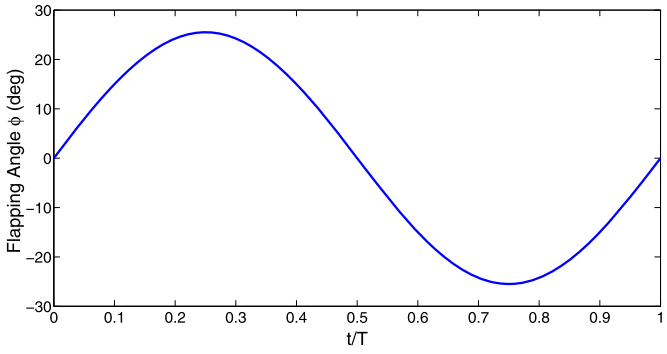

(a) Optimum flapping angle φ

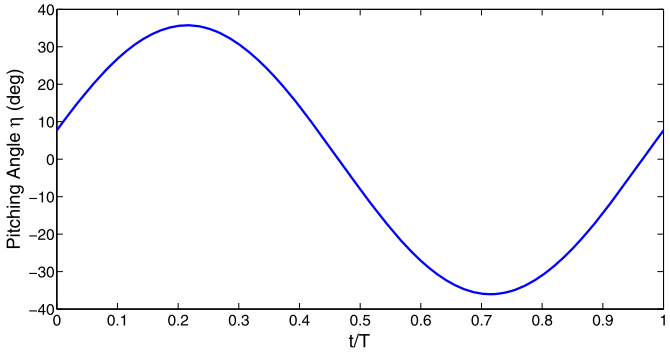

(b) Optimum flapping angle η

Fig. 11. Optimal kinematic functions using full unsteady model.

phase shift of the Theodorsen function. Hence, they showed that the unsteady aerodynamics of hovering insects result in a magnitude drop of 0.64–0.75 in the generated lift from the quasi-steady calculations. As such, the kinematics obtained by quasi-steady models is not sufficient to produce the required lift when used in an unsteady model. Hence, optimization using unsteady models requires more flapping than their quasi-steady counterparts to satisfy the same lift equality constraint. This is shown in Table 1 as the flapping amplitude increases from 18.9° to 25.5° and the pitching amplitude increases from 29.2° to 35.9° when comparing the full quasi-steady results to the full unsteady ones.

6. Sensitivity analysis

In this section, a sensitivity analysis for the variations of the cost function (normalized power P^*) and the lift constraint with all of the seven design variables is performed. Figs. 12–18 show the variations of P^* and L^* with each of design variables where the other design variables are held constant at the optimal values. As expected, the lift constraint is active.

Fig. 12 shows typical monotonic cubic and quadratic behaviors for power and lift variations with frequency. The optimum value was determined to satisfy the lift constraint. Similar behaviors are noted in the cases of flapping and pitching amplitudes, as shown in Figs. 13 and 14, respectively. A different behavior is observed for P^* and L^* with the mean pitching angle η_0, as shown in Fig. 15.

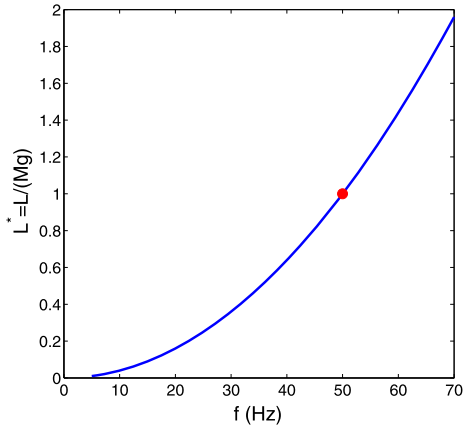

(a) Lift-to-weight ratio L^*

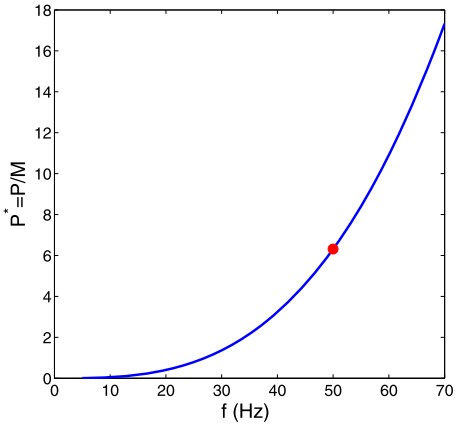

(b) Normalized power P^*

Fig. 12. Variations of the normalized power and the lift-to-weight ratio with the flapping frequency where the other design variables are set to their optimal values, using full unsteady representations as shown in Table 1. The red point represents the optimum points. (For interpretation of the references to color in this figure legend, the reader is referred to the web version of this article.)

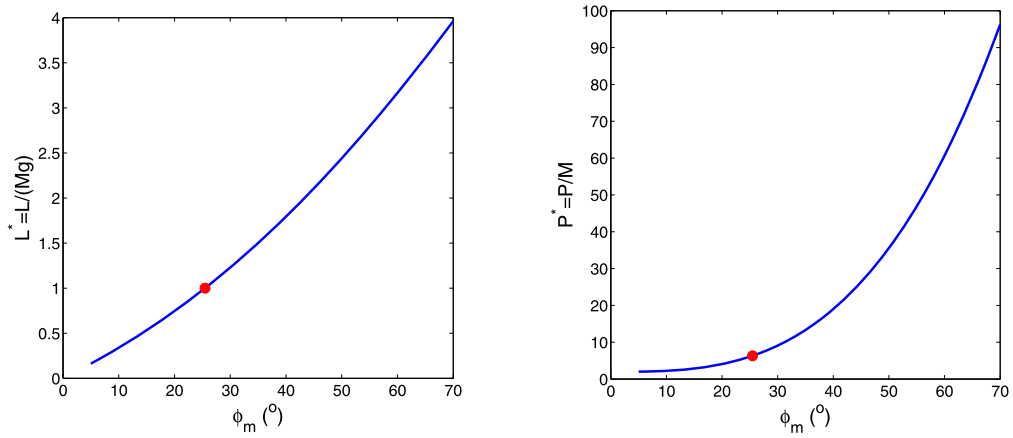

(a) Lift-to-weight ratio L^* (b) Normalized power P^*

Fig. 13. Variations of the normalized power and the lift-to-weight ratio with the flapping amplitude where the other design variables are set to their optimal values, using full unsteady representations as shown in Table 1. The red point represents the optimum points. (For interpretation of the references to color in this figure legend, the reader is referred to the web version of this article.)

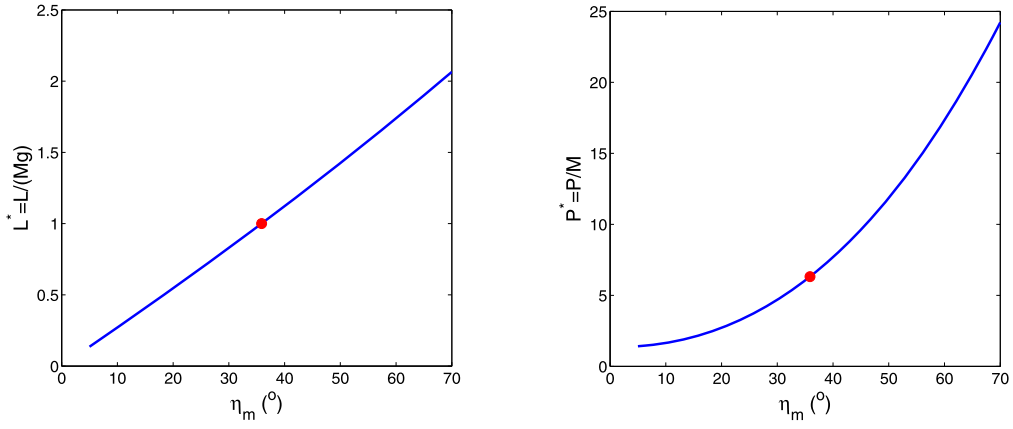

(a) Lift-to-weight ratio L^* (b) Normalized power P^*

Fig. 14. Variations of the normalized power and the lift-to-weight ratio with the pitching amplitude where the other design variables are set to their optimal values, using full unsteady representations as shown in Table 1. The red point represents the optimum points. (For interpretation of the references to color in this figure legend, the reader is referred to the web version of this article.)

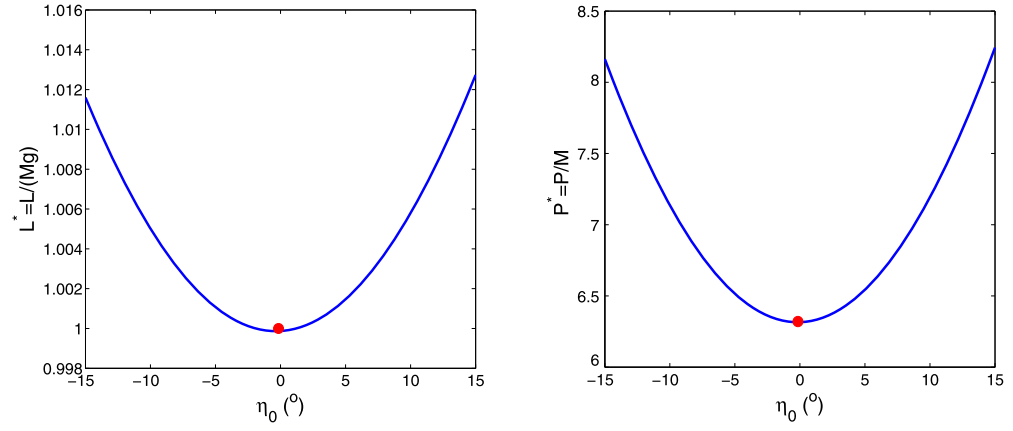

(a) Lift-to-weight ratio L^* (b) Normalized power P^*

Fig. 15. Variations of the normalized power and the lift-to-weight ratio with the mean pitch angle where the other design variables are set to their optimal values, using full unsteady representations as shown in Table 1. The red point represents the optimum points. (For interpretation of the references to color in this figure legend, the reader is referred to the web version of this article.)

The optimizer could find a local minimum for the required aerodynamic power around almost zero mean pitching angle, at which the other parameters (e.g., frequency and motion amplitudes) are set to satisfy the lift constraint. As for K (control parameter of the flapping motion), there are two values to satisfy the lift constraint, as shown in Fig. 16. The optimizer converged to the lower value because of the corresponding lower power. In fact, the lower K-value is selected for all of the four cases including rotational

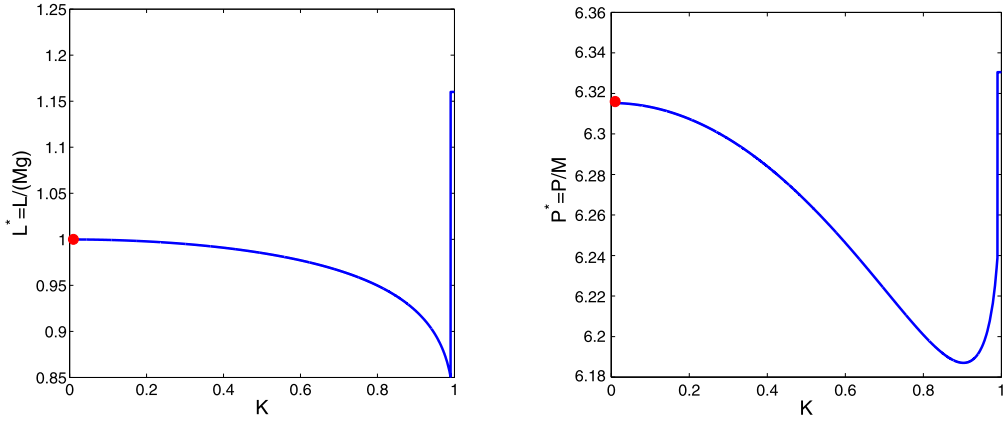

(a) Lift-to-weight ratio L^* (b) Normalized power P^*

Fig. 16. Variations of the normalized power and the lift-to-weight ratio with the control parameter for flapping motion K where the other design variables are set to their optimal values, using full unsteady representations as shown in Table 1. The red point represents the optimum points. (For interpretation of the references to color in this figure legend, the reader is referred to the web version of this article.)

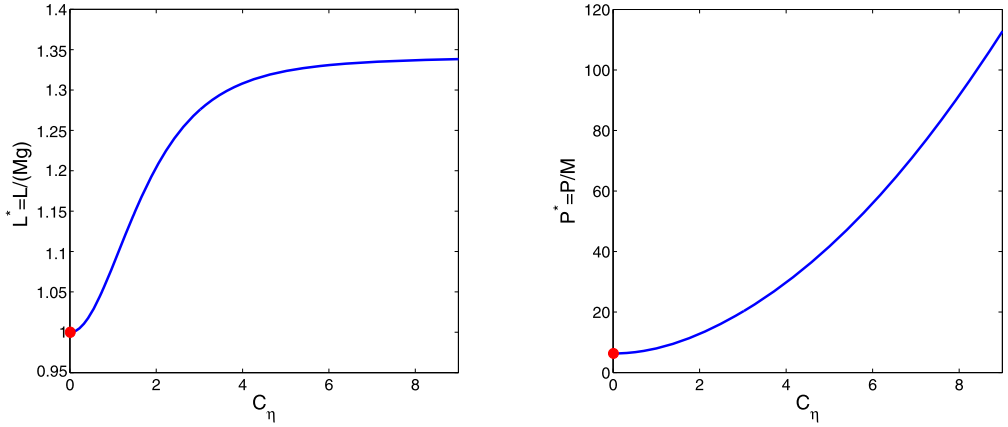

(a) Lift-to-weight ratio L^* (b) Normalized power P^*

Fig. 17. Variations of the normalized power and the lift-to-weight ratio with the control parameter for pitching motion C_η where the other design variables are set to their optimal values, using full unsteady representations as shown in Table 1. The red point represents the optimum points. (For interpretation of the references to color in this figure legend, the reader is referred to the web version of this article.)

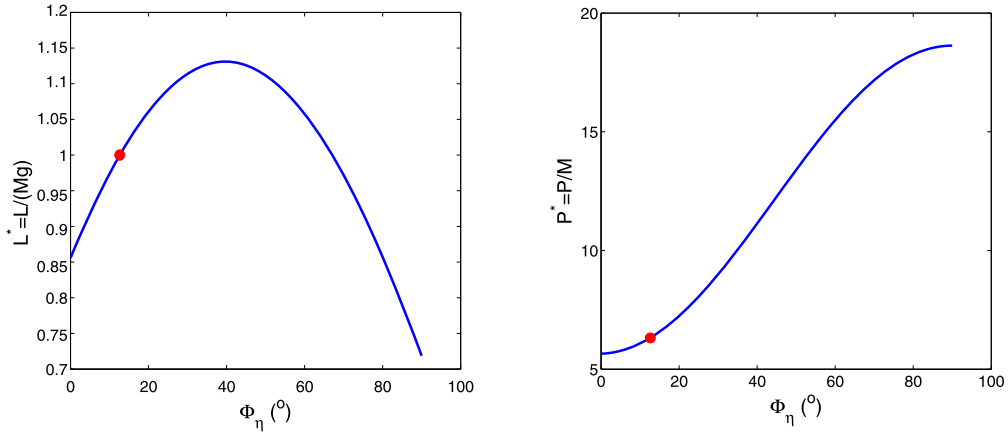

(a) Lift-to-weight ratio L^* (b) Normalized power P^*

Fig. 18. Variations of the normalized power and the lift-to-weight ratio with the flapping-pitching phase angle where the other design variables are set to their optimal values, using full unsteady representations as shown in Table 1. The red point represents the optimum points. (For interpretation of the references to color in this figure legend, the reader is referred to the web version of this article.)

contributions, as shown in Table 1. Luckily, the optimizer could find another local minimum for P^* at the boundary of C_η-variation (zero), as shown in Fig. 17. Similar to the K-case, the smooth variations are preferred by the optimizer for their considerably lower required aerodynamic power. Finally, the optimum phase angle is determined to satisfy the lift constraint, despite of the local min-

imum around 0°, as shown in Fig. 18. In summary, two types of optimal values are found. The first set includes the mean pitch angle η_0 and the control parameter for pitch motion C_η. Clear local power minima are found with these design variables. The other design variables (frequency, amplitudes, and phase shift) are then set to satisfy the lift constraint.

7. Conclusion

Optimization of wing-kinematics for hovering micro-air-vehicles is considered by projecting the problem down to a finite dimensional space of design variables. These design variables represent the parameters for some specific kinematic functions. Four aerodynamic models having different levels of fidelity and captured physical aspects were used to assess the effects of the aerodynamic model on the optimal wing kinematics. Each model has an additive physical aspect that was not included in the previous one to specifically assess the effect of this added aspect on the optimization problem. These physical aspects are the leading edge vortex, the rotational lift, the non-circulatory contributions, and the unsteadiness.

The quasi-steady representation for the leading edge vortex yielded a triangular waveform for the back and forth flapping angle and piece-wise constant pitching angle; the same result obtained in a previous effort using calculus of variations. Incorporating a potential flow model to the rotational contributions resulted in total dependence on rotational motions as a source of lift; 7° flapping amplitude versus the 180° pitching amplitude. Adding viscous rotational power, more reasonable kinematics were obtained. However, the optimizer remained dependent on the rotational motion. This is because the rotational motion creates lift with very little power consumption in comparison to the translational motion. As such, the optimum normalized power was reduced from 19.52 W/kg to 3.22 W/kg. Adding the non-circulatory components, along with the assumption of 100% elastic storage, does not lead to a considerable change in the optimal kinematics. Finally, using the full unsteady model resulted in higher values for the minimum required mechanical power. That is, optimization of flapping kinematics using quasi-steady aerodynamics lead to less conservative results.

Conflict of interest statement

The authors declare that there is no conflict of interests regarding the publication of this article.

References

[1] A. Andersen, U. Pesavento, Z. Wang, Unsteady aerodynamics of fluttering and tumbling plates, J. Fluid Mech. 541 (2005) 65–90.
[2] A. Andersen, U. Pesavento, Z.J. Wang, Analysis of transitions between fluttering, tumbling and steady descent of falling cards, J. Fluid Mech. 541 (2005) 91–104.
[3] G.J. Berman, Z.J. Wang, Energy-minimizing kinematics in hovering insect flight, J. Fluid Mech. 582 (2007) 153–168.
[4] R.L. Bisplinghoff, H. Ashley, R.L. Halfman, Aeroelasticity, Dover Publications, New York, 1996.
[5] T. Cebeci, M. Platzer, H. Chen, K.C. Chang, J.P. Shao, Analysis of Low Speed Unsteady Airfoil Flows, Horizons Publishing Inc./Springer, Long Beach/Berlin, Heidelberg, New York, 2005.
[6] R. Demoll, Der Flug der Insekten und der Vogel, G. Fischer, Jena, 1918.
[7] R. Demoll, Der Flug der Insekten, Naturewissenschaften 7 (1919) 480–481.
[8] M.H. Dickinson, F.-O. Lehmann, S.P. Sane, Wing rotation and the aerodynamic basis of insect flight, Science 284 (1999) 1954–1960.
[9] D.B. Doman, M.W. Oppenheimer, D.O. Sigthorsson, Wingbeat shape modulation for flapping-wing micro-air-vehicle control during hover, J. Guid. Control Dyn. 33 (2010) 724–739.
[10] C.P. Ellington, The aerodynamics of hovering insect flight: III. Kinematics, Philos. Trans. R. Soc. Lond., Ser. B 305 (1984) 41–78.
[11] C.P. Ellington, The aerodynamics of hovering insect flight: II. Morphological parameters, Philos. Trans. R. Soc. Lond., Ser. B 305 (1984) 17–40.
[12] C.P. Ellington, C. Van den Berg, A.P. Willmott, A.L.R. Thomas, Leading-edge vortices in insect flight, Nature 384 (1996) 626–630.
[13] Y.C. Fung, An Introduction to the Theory of Aeroelasticity, Dover, New York, 1969.
[14] M. Ghommem, M.R. Hajj, D.T. Mook, B.K. Stanford, P.S. Beran, R.D. Snyder, L.T. Watson, Global optimization of actively morphing flapping wings, J. Fluids Struct. 33 (2012) 210–228.
[15] R.T. Jones, Operational treatment of the nonuniform lift theory to airplane dynamics, Tech. Rep. 667, NACA, 1938.
[16] M. Kurdi, B. Stanford, P. Beran, Kinematic optimization of insect flight for minimum mechanical power, AIAA paper 2010-1420, 2010.
[17] M.W. Oppenheimer, D.B. Doman, D.O. Sigthorsson, Dynamics and control of a biomimetic vehicle using biased wingbeat forcing functions, J. Guid. Control Dyn. 34 (2011) 204–217.
[18] U. Pesavento, Z.J. Wang, Navier–Stokes solutions, model of fluid forces, and center of mass elevation, Phys. Rev. Lett. 93 (2004).
[19] E.C. Polhamus, A concept of the vortex lift of sharp-edge delta wings based on a leading-edge-suction analogy, Tech. Rep. NASA TN D-3767, Langely Research Center, Langely Station, Hampton, Va, 1966.
[20] L. Schenato, D. Campolo, S.S. Sastry, Controllability issues in flapping flight for biomimetic MAVs, in: 42nd IEEE Conference on Decision and Control, 2003, pp. 6441–6447.
[21] B.K. Stanford, P.S. Beran, Analytical sensitivity analysis of an unsteady vortex-lattice method for flapping-wing optimization, J. Aircr. 47 (2010) 647–662.
[22] H.E. Taha, M.R. Hajj, A.H. Nayfeh, Flight dynamics and control of flapping-wing MAVs: a review, Nonlinear Dyn. 70 (2012) 907–939.
[23] H.E. Taha, M.R. Hajj, A.H. Roman, A.H. Nayfeh, A calculus of variations approach for optimum maneuverability of flapping MAVs near hover, J. Guid. Control Dyn. 37 (2014) 167–1372.
[24] H.E. Taha, M.R. Hajj, A.H. Nayfeh, Wing kinematics optimization for hovering micro air vehicles using calculus of variation, J. Aircr. 50 (2013) 610–614.
[25] H.E. Taha, M.R. Hajj, P.S. Beran, State space representation of the unsteady aerodynamics of flapping flight, Aerosp. Sci. Technol. 34 (2014) 1–11.
[26] H.E. Taha, M.R. Hajj, P.S. Beran, Unsteady nonlinear aerodynamics of hovering MAVs/insects, AIAA paper 2013-0504, 2013.
[27] T. Theodorsen, General theory of aerodynamic instability and the mechanism of flutter, Tech. Rep. 496, NACA, 1935.
[28] C. Van den Berg, C.P. Ellington, The vortex wake of a hovering model hawkmoth, Philos. Trans. R. Soc. Lond., Ser. B 352 (1997) 317–328.
[29] C. Van den Berg, C.P. Ellington, The three-dimensional leading-edge vortex of a hovering model hawkmoth, Philos. Trans. R. Soc. Lond., Ser. B 352 (1997) 329–340.
[30] Z.J. Wang, J.M. Birch, M.H. Dickinson, Unsteady forces in hovering flight: computation vs experiments, J. Exp. Biol. 207 (2004) 449–460.
[31] T. Weis-Fogh, Quick estimates of flight fitness in hovering animals, including novel mechanisms for lift production, J. Exp. Biol. 59 (1973) 169–230.